Impact of rain cell on scatterometer data: 2. Correction of Seawinds measured backscatter and wind and rain flagging

J. Tournadre and Y. Quilfen

Laboratoire d'Océanographie Spatiale, Institut Français de Recherche pour l'Exploitation de la Mer, Plouzané, France

Received 15 October 2004; revised 16 March 2005; accepted 12 April 2005; published 28 July 2005.

[1] Rain can strongly modify the normalized radar cross section (NRCS) measured by Ku-band scatterometers and alter the wind vector retrieval. Part 1 of this paper (Tournadre and Quilfen, 2003) presented a theoretical model of interaction between rain and scatterometer signal and used it to quantify the effect of rain on the backscatter and on wind vectors. Their results showed that the scatterometer data are strongly affected by rain, that they are extremely sensitive to the rain distribution within scatterometer resolution cells, and that the normalized radar cross section (NRCS) variability induced by rain could be a good indicator for rain flagging. The model is further tested and validated on a tropical cyclone case using colocated high resolution rain and Seawinds NRCS data. The model is used to compute attenuation and volume scattering from Tropical Rainfall Mapping Mission Precipitation Radar (TRMM PR) rain data. The comparison of the high-resolution (4 km) NRCS to synthetic NRCS computed from National Hurricane Center (NHC) winds and modeled rain terms shows a good qualitative agreement. The rain terms are used to correct the measured NRCS, to infer corrected winds which are significantly improved compared to NHC winds, especially for high winds. The wind correction using low-resolution rain data (such as Special Sensor Microwave Imager (SSM/I) ones) is also investigated using rain data averaged over wind scatterometer cells. This can also significantly improve the rain retrieval. A new rain flag based on the NRCS variability within wind vector cells is presented and shown to perform better than the operational one.

Citation: Tournadre, J., and Y. Quilfen (2005), Impact of rain cell on scatterometer data: 2. Correction of Seawinds measured backscatter and wind and rain flagging, *J. Geophys. Res.*, *110*, C07023, doi:10.1029/2004JC002766.

1. Introduction

[2] The two scatterometers recently in operation, Seawinds on QuikScat and AMI-wind on ERS-2, were designed to measure the wind speed and direction over the global ocean. They both employ radars, at Ku-band (13.4 GHz) for Seawinds and at C-band (5.6 GHz) for AMI-WIND, to measure the sea surface backscatter at multiple azimuths, incidences and polarizations from which wind speed and direction are inferred using semi-empirical models. These two sensors provide a good coverage of the ocean and their wind products are of great value for the ocean and meteorological communities. The accuracy of the ocean winds estimated from scatterometer backscatter measurements is influenced to varying degrees by rain. In a previous paper, *Tournadre and Quilfen* [2003] (hereinafter TQ) presented a theoretical model of interaction between rain and scatterometer data. On the basis of radiative transfer formulation, this model includes attenuation and volume scattering by raindrops. The modification of surface roughness by impinging drops was not considered because of the lack of reliable parameterization of this effect.

[3] Using analytical rain cell models and constant surface backscatter or wind fields, the modification by rain of the measured backscatter and of the retrieved wind vectors was estimated for Ku-band (Seawinds) and C-band (AMI-Wind) scatterometers. The modeling results at Ku-band show that scattering by raindrops plays a major role at low normalized radar cross section (NRCS), resulting in a signal enhancement, and that attenuation predominates for high NRCS. Even rain rates as low as 1 mm hr^{-1} can modify the NRCS by several dB. The detailed analysis of the NRCS modification within rain cells and scatterometer cells revealed a stronger NRCS dependency on the distribution of rain within the scatterometer cell than on the average rain rate.

[4] The effect of rain on the wind retrieval is more complex as it involves NRCS measurements at different incidences, azimuths, and polarizations and as the rain influence strongly depends on the surface NRCS. Because of the shape of the KMOD model function, the error induced by rain on wind speed follows a similar trend as

0148-0227/05/2004JC002766$09.00

the one on NRCS, i.e., an overestimation of low winds and an underestimation of high winds. The wind direction retrieval is affected in a complex manner. It depends more strongly on the rain rate distribution within the scatterometer resolution cell than on any other parameter (average rain rate, wind speed). No general trend can really be determined and the dispersion around the mean values is so high that the retrieved wind direction can almost be considered as a random variable.

[5] The inversion of the rain-affected NRCS showed that the Maximum Likelihood Estimator (MLE) has often values within the limit defined for quality control and can thus hardly efficiently detect rain-affected samples. The analysis showed that the strong nonlinearity of the rain influence and the inhomogeneous nature of rain within the scatterometer cell induce large NRCS variability within wind vector cells. NRCS variability could therefore be a possible candidate for rain flagging. The results of the theoretical study have to be further tested and assessed on real scatterometer and rain data to better understand the influence of rain on the NRCS and on the wind retrieval, and to analyze the feasibility of the winds correction in the presence of rain, as well as to test the efficiency of a rain flag based on the NRCS variability.

[6] Because the distribution of rain within the scatterometer wind retrieval cell is one of the most important factors in estimating the influence of rain on scatterometer data, as shown by TQ, it is essential to conduct this study to have not only high-resolution rain data, i.e., at a finer resolution than the standard scatterometer wind vector cell, but also to have high-resolution surface NRCS such as the ones recently defined by *Spencer et al.* [2000, 2003] and *Early and Long* [2001].

[7] The second part of the paper presents a direct assessment of the rain effects on Ku-band scatterometer data using colocated Tropical Rainfall Mapping Mission Precipitation Radar (TRMM PR) precipitation data and Seawinds Scatterometer Image Reconstruction (SIR) high resolution NRCS data [*Spencer et al.*, 2000; *Early and Long*, 2001] during a tropical cyclone event (Floyd). Tropical cyclones are certainly extreme situations which associate heavy rains and high winds. In general, almost all Seawinds data are flagged by the operational rain flag and few valid data can be used to study the distribution of winds within tropical cyclones. However, scatterometer wind fields could potentially be a powerful tool to improve our knowledge of TC if the influence of rain on the retrieved wind vectors could be corrected. It is thus important to investigate the feasibility of a correction of the wind vectors in such situations. It is also of importance to define a rain flag which can discriminate between rain and no rain samples but also between samples that can or cannot be corrected for rain.

[8] In the following section, we provide the necessary background regarding the rain/scatterometer interaction model. Section 3 presents the data used in this study, i.e., Seawinds on QuikScat scatterometer data, TRMM rain rate data, and National Hurricane Center wind fields. Section 4 briefly describes the TC Floyd. Section 5 analyzes the rain effects using the rain-scatterometer interaction model and presents the correction of NRCS and wind fields using high-resolution and low-resolution rain data. Section 6 analyzes the operational Seawinds rain flags and proposed a new flag based on the NRCS variability estimated from Seawinds slices data.

2. Rain/Scatterometer Interaction Model

[9] The model of rain/scatterometer signal interaction has been described in detail in TQ and will only be briefly described in this section. Within a rain cell over the ocean, the scatterometer radar signature is composed of contributions from volume scattering and attenuation by raindrops in the atmosphere as well as from surface scattering by sea surface roughness. The sea surface roughness depends mainly on the surface wind but is also modified by raindrops impinging on the sea surface. Raindrops generate ring waves which enhance the sea surface roughness [*Moore et al.*, 1997; *Bliven et al.*, 1997; *Craeye and Schlüssell*, 1998], but they also generate turbulence in the upper water layer which attenuates the short surface waves [*Nystuen*, 1990; *Tsimplis*, 1992]. The analysis of SIR-C/X-SAR Synthetic Aperture Radar data by *Melsheimer et al.* [1998] has shown that the rain modification of the sea surface roughness depends strongly on the wavelength of the water waves. The net effect on the sea surface is a decrease of the amplitude of those water waves which have wavelengths above 10 cm and a decrease of the amplitude of those water waves which have wavelengths below 5 cm. Unfortunately, the critical wavelength at which the increase of the wave amplitude turns into a decrease is not well defined. It depends on the rain rate, the drop size distribution, the wind speed, and the temporal evolution of the rain event. A recent study by *Contreras et al.* [2003] analyzed the effect of rain on Ku-band backscatter using a ship-borne radar system. They found that at Seawinds incidence angles, rain increases the backscatter, at least for low wind speed ($\leq$10 m s^{-1}). More recently, *Draper and Long* [2004] evaluated the effect of rain on Seawinds measurements using colocated TRMM rain data and numerical model wind data. They proposed a parameterization of the surface modification by rain in the form of a polynomial of the rain rate. As stated by the authors, above 10 km mm hr^{-1} rain, atmospheric attenuation and volume scattering dominate the signal and it is thus difficult to estimate any surface roughness modification. Tests conducted using their parameterization showed only a slight modification (less than 0.2 dB) of the modeled NRCS for winds above 10 m s^{-1}. The lack of a reliable parameterization for moderate to high rain rate and high winds lead us not to consider the modification of the surface roughness by rain in the model. It should be noted that such modification can easily by included in the model if a parameterization becomes available.

[10] In the presence of rain, the backscatter from all hydro-meteors that have the same range to the sensor are mapped onto the same radar range bin [*Melsheimer et al.*, 1998]. This contribution from volume backscatter, which is also affected by attenuation due to the presence of rain in the atmosphere, is added to the contribution from backscatter at the sea surface. Using the results from *Melsheimer et al.* [1998], TQ showed that, assuming a cylindrical rain cell of diameter d and height h and constant rain rates along the tilted path lengths, the

effective NRCS, $\widetilde{\sigma_0}$, for a point $M(x, y)$ of the ocean surface is given by

$$\widetilde{\sigma}_0(x,y) = \sigma_0(x,y)e^{-2k_a(x,y)f_y(0)} + \frac{\sin\theta}{2}\int_0^{l(y)} \eta(s)\frac{1}{k_a(s)}e^{-2f_y(s)k_a(s)}ds, \quad (1)$$

where σ_0 is the surface NRCS, η is the volume backscatter coefficient, k_a is the attenuation coefficient, θ is the incidence angle, y is the ground range coordinate, $l(y)$ is the length of the rain filled tilted column contributing to the effective NRCS, $f_y(s)$ is the boundary of the rain cell as a function of the coordinate s of the tilted column with the origin at y, and $f_y(0)$ is the path length of radar signal at range y. TQ showed that $l(y)$ and $f_y(s)$ have the following form:

$$l(y) = \min\left(\max\left(0,\frac{y_2 - y}{\cos\theta}\right),\frac{h}{\sin\theta}\right) - \min\left(\max\left(0,\frac{y_1 - y}{\cos\theta}\right),\frac{h}{\sin\theta}\right) \quad (2)$$

$$f_y(s) = f_1(s) - f_2(s), \quad (3)$$

where

$$f_1(s) = \min\left(\max\left(0,\frac{s - s_1}{\tan\theta}\right), le_y(s)\right) \quad (4)$$

$$f_2(s) = \min\left(\max\left(0,\frac{s - s_2}{\tan\theta}\right), le_y(s)\right) \quad (5)$$

$$le_y(s) = -\tan\theta s + \frac{h}{\cos\theta}, \quad (6)$$

le_y, f_1, and f_2 represent the equations of the rain cell boundaries in the local coordinate system and $s = (y - y_0)/\cos\theta$. Here y_1, y_2, s_1, and s_2 represent the ordinates of the rain cell inner and outer edges.

[11] Attenuation, k_a, depends on rain rate, R, by [*Marshall and Palmer*, 1948]

$$k_a = 2aR^b, \quad (7)$$

where a and b are frequency dependent coefficients. At Ku-band (13.4 GHz), the a and b coefficients are, respectively, 0.0314 and 1.14 [*Slack et al.*, 1994]. The volume scattering η is given by *Ulaby et al.* [1981],

$$\eta = \frac{\pi^5}{\lambda_0^4}10^{-18}|K_0|^2 400R^{1.4}, \quad (8)$$

where λ_0 denotes the radar wavelength and K_0 is a quantity which describes the scattering efficiency of the hydrometeors. This model, designed primarily to test the influence of analytical rain cells, can be easily adapted to any rain fields, such as the ones measured by TRMM, by assuming a cylindrical rain cell of infinite diameter. Under this assumption, f_y and l simplify to

$$l(y) = \frac{h}{\sin\theta} \quad (9)$$

$$f_y(s) = -\tan\theta s + \frac{h}{\cos\theta}, \quad (10)$$

and the modified NRCS reduces to

$$\widetilde{\sigma}_0(x,y) = \sigma_0(x,y)e^{-2\frac{k_a(x,y)h}{\cos\theta}} + \frac{\sin\theta}{2}\int_0^{\frac{h}{\sin\theta}} \eta(s)\frac{1}{k_a(s)}e^{-2k_a(s)\left(-\tan\theta s + \frac{h}{\cos\theta}\right)}ds \quad (11)$$

or

$$\widetilde{\sigma}_0(x,y) = A(x,y)\sigma_0(x,y) + \sigma_{vol}(x,y), \quad (12)$$

where A and σ_{vol} are the rain attenuation and the emission defined by

$$A(x,y) = e^{-2\frac{k_a(x,y)h}{\cos\theta}} \quad (13)$$

$$\sigma_{vol}(x,y) = \frac{\sin\theta}{2}\int_0^{\frac{h}{\sin\theta}} \eta(s)\frac{1}{k_a(s)}e^{-2k_a(s)\left(-\tan\theta s + \frac{h}{\cos\theta}\right)}ds. \quad (14)$$

3. Data

3.1. Seawinds on QuikScat Scatterometer Data

[12] The Seawinds instrument on board QuikScat and ADEOS II is a pencil-beam scanning scatterometer operating at Ku-band (13.46 GHz). It uses a 1-m-diameter rotating disk that produces two spot beams, sweeping in a circular pattern. The incidence angles are 46° and 54° for the inner and outer beams, respectively. The inner and outer beams are horizontal and vertical polarizations, respectively. Each 25×25 km^2 ground cell used in the wind retrieval is sampled between 8 and 15 times. The azimuth angles of these samples are not independent but correspond to four distinct narrow ranges of azimuth angles from the forward and aft halves of the antenna rotation and for each beam. These azimuth angles are determined by the position of the satellite and by the antenna incidence angle, θ. Taking into account the Earth curvature, the ground range distance, r_a, and the azimuth ψ are given by

$$r_a = \frac{H}{\cos(\theta)} + \frac{H^2}{2a}\tan^2(\theta) \quad (15)$$

$$\psi = \mp arccos\left(\frac{y}{r_a}\right). \quad (16)$$

Recently, *Spencer et al.* [2000, 2003] and *Early and Long* [2001] developed an improved resolution backscatter measurement for the Seawinds pencil-beam scatterometer

using the Scatterometer Image Reconstruction (SIR) algorithm [*Early and Long*, 2001]. D. Long (personal communication, 2004) provided us with the high-resolution SIR backscatter data necessary for this study. These SIR NRCS data have a nominal pixel resolution of 2.225 km with an estimated effective resolution of about 4 km. For each antenna, i.e., for each incidence angle, forward-looking and an aft-looking fields are produced.

3.2. TRMM

[13] The Tropical Rain Mapping Mission (launched in November 1997) is a joint mission of NASA and National Space Development Agency (NASDA). The objectives of TRMM are to measure rainfall and energy (latent heat of condensation) exchange in the tropical and subtropical regions of the globe. The primary rainfall instruments on board TRMM are the TRMM microwave imager (TMI), the precipitation radar (PR), and the Visible and Infrared Radiometer System (VIRS). The primary objective of the PR, which is the first rain radar in space, is to provide the three-dimensional structure of rainfall. It is a 128-element active phase array system operating at Ku-band (13.8 GHz). It sends radar pulses and measures the backscatter from the atmosphere. The three-dimensional rainfall distribution is inferred from the radar reflectivity. PR has a horizontal ground resolution of about 4 km and a swath width of 220 km. It provides vertical profiles of the rain from the surface up to a height of about 20 km. PR is able to separate out rain echoes for vertical sample sizes of about 250 m at nadir [*Kummerow et al.*, 1998].

3.3. National Hurricane Center Wind Data

[14] The Hurricane Research Division (HRD) wind analysis requires the input of all available surface weather observations (e.g., ships, buoys, coastal platforms, surface aviation reports, reconnaissance aircraft data adjusted to the surface). This includes the QuikScat data. Depending on the quality control performed on these data (especially on the rain flags), the analysis is more or less dependent on QuikScat. All data are processed to conform to a common framework for the averaging time period. The analysis provides thus the maximum sustained 1-min wind speed. As seen, it enables clear featuring of the wind speed structures, i.e., the low wind speed center and the maximum wind area and radius locations with the maximum wind occurring on the right side of the moving cyclone. However, because of the poor coverage of the aircraft flights and the smoothing effect of the analysis process, many details of the surface winds are probably filtered out. Indeed, systematic wind patterns associated with the convection areas have been documented, but are obviously missing in the HRD wind analysis.

4. Tropical Cyclone Floyd

[15] The following description of Floyd is based on the reports produced by the National Hurricane Center (NHC) of the National Oceanic and Atmospheric Administration [http://www.nhc.noaa.gov]. Floyd was a large and intense Cape Verde hurricane that pounded the central and northern Bahamas islands, seriously threatened Florida, struck the coast of North Carolina, and moved up the United States east coast into New England. It neared the threshold of category 5 intensity on the Saffir/Simpson Hurricane Scale as it approached the Bahamas, and produced a flood disaster of immense proportions in the eastern United States, particularly in North Carolina.

[16] Floyd can be traced back to a tropical wave that emerged from western Africa on 2 September. The wave proceeded westward across the eastern tropical Atlantic for several days. The cloud pattern became sufficiently well organized for the system to become Tropical Storm Floyd on 8 September. Floyd slowly strengthened and became a hurricane on 10 September while taking a northwestward motion. After strengthening nearly to category 3 status early on 11 September, the hurricane weakened to 85 knots around 0000 UTC on 12 September. Early on 12 September a westward turn marked the beginning of a major strengthening episode. Maximum sustained winds increased from 95 knots to 135 knots, and the central pressure fell about 40 mb from early on 12 September to early on 13 September. From 0600 UTC to 1800 UTC on 13 September, Floyd was at the top end of category 4 intensity on the Saffir/Simpson Hurricane Scale. Floyd was aimed at the central Bahamas until late on 13 September, when the heading became west-northwestward. Floyd continued to turn gradually to the right, the center of the hurricane paralleling the central Florida coast. Floyd intensity diminished from 13 to 15 September. After turning toward the north-northeast with forward speed increasing to near 15 knots, Hurricane Floyd made landfall near Cape Fear, North Carolina, at 0630 UTC on 16 September as a category 2 hurricane with estimated maximum winds near 90 knots.

[17] During its lifetime, Floyd was observed several times by QuikScat and TRMM. The best colocation in time and space of surface winds and rain fields was obtained on 13 September when Floyd was sampled at 1048 UT by Seawinds and at 1006 UT by TRMM. Figure 1 presents the TRMM VIRS channel 3 data and the Seawinds winds vectors (level 2B data) for the colocated data. The best track from NHC has also been overlaid on the plot. Figure 1 presents the analysis of surface wind field at 1330 UT made by the Hurricane Research Division (HRD) of the AOML (available at http://www.aoml.noaa.gov/hrd/Storm_pages/).

5. Correction of the NRCS and Wind Fields

[18] As already mentioned, the influence of rain strongly depends on the rain distribution within the scatterometer resolution cell. An accurate estimate of the rain influence on scatterometer thus requires the availability of rain rate and NRCS fields at similar resolution. In a first step, the validity of the rain/scatterometer interaction model is tested by comparing the measured Long high resolution (HR) SIR NRCS to NRCS modeled using the TRMM rain fields and the surface NRCS inferred from high-resolution NHC wind fields. The correction of the HR NRCS using the rain model is then presented. As the operational scatterometer wind retrieval cell is typically of 25×25 km^2, the correction of the mean NRCS averaged over the wind retrieval cell is also studied.

[19] In general, high-resolution rain data such as the TRMM ones are not available to correct for the rain influence. However, rain estimates at a resolution similar

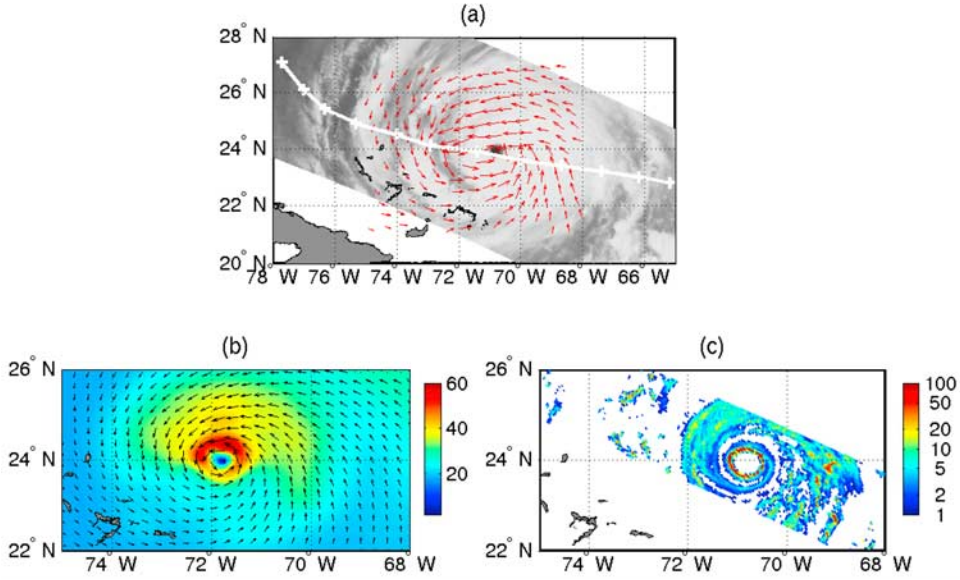

Figure 1. (a) Hurricane Floyd revealed by wind vectors from Seawinds (1048 UT) and TRMM VIRS imager (channel 4)(1006 UT) on 23 September 1999. (b) National Hurricane Center HRD surface wind field at 1330 UT on 13 September 1999. (c) Average rain rate from the TRMM precipitation radar at 1006 UT 13 September 1999.

to that of the wind retrieval can be quite easily obtained from passive radiometers (such as AMSR on board ADEOS2 or coincident SSM/I data). It is thus important to have an insight on the capability and pertinence of a NRCS correction using these low-resolution rain rate fields. This is done using the TRMM rain fields by comparing the high-resolution correction averaged over a wind resolution cell to the correction estimated from the rain rate averaged over the same scatterometer cell. The rain-corrected NRCS are then used to infer rain-corrected wind fields.

5.1. Validation of the Rain Interaction Model Using High-Resolution NRCS

[20] Figure 2 presents the Seawinds high resolution SIR NRCS fields, resampled on the TRMM grid over TC Floyd on 13 September 1048 UT. The influence of rain is clearly

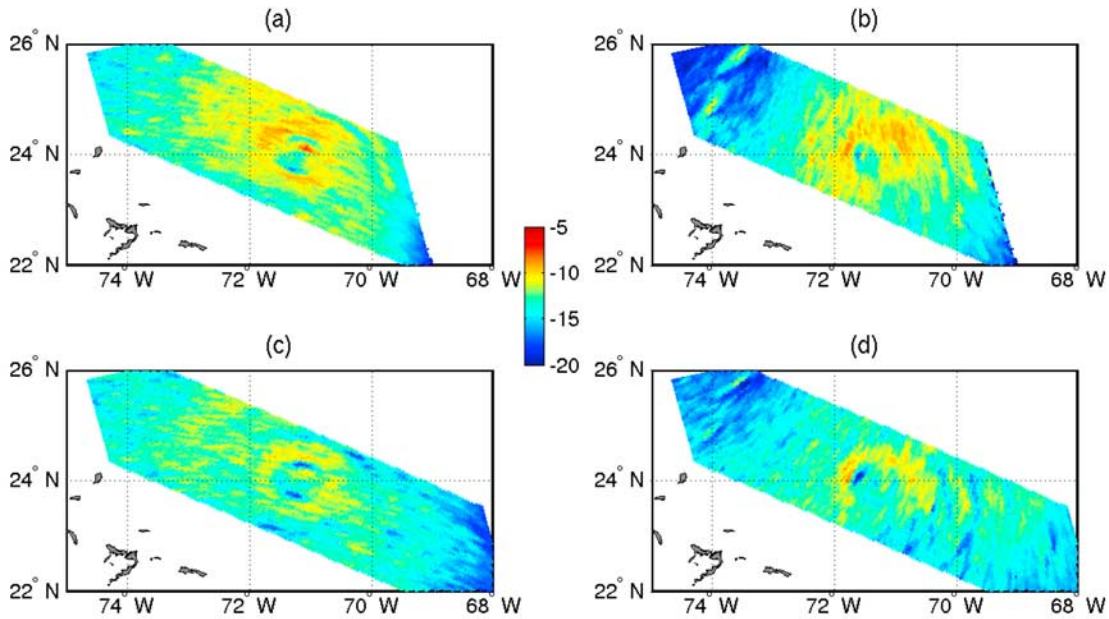

Figure 2. High-resolution Seawinds NRCS for the inner and outer antennae gridded at 2.5 km resolution (D. G. Long, personal communication, 2004) 1048 UT 13 September 1999. (a) Inner antenna forward look, (b) inner antenna aft look, (c) outer antenna forward look, and (d) outer antenna aft look.

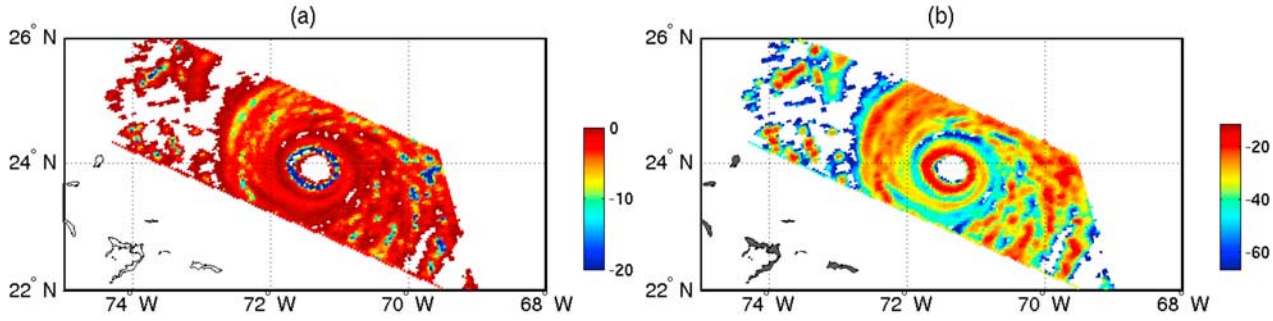

Figure 3. (a) Modeled attenuation $A(x, y)$ and (b) volume scattering from TRMM PR (Figure 1c) data using equations (13) and (14) for the inner antenna and the forward look.

visible on these fields in the alternation of bands of high and low backscatter associated with the TC rain patterns presented in Figure 1c. In the region of maximum rain rate (over 30 mm hr^{-1}) near the eyewall, rain attenuation is so strong that the measured NRCS are lower than those within the TC eye itself where there is no rain and where wind is low. As the TC moves rapidly and as precipitation patterns within TC constantly evolves, the rain field certainly changed during the 30 min time lag between the QuikScat and TRMM passes. In a first step, we test the validity of the rain/scatterometer interaction model by forward modeling, i.e., by comparing the measured HR NRCS and the NRCS modeled using the TRMM rain field and a surface NRCS inferred from the high-resolution NHC wind fields.

[21] The rain volume emission and attenuation terms are first computed for each antenna and for each azimuth (forward and aft looks) using equations (13) and (14) at the 4-km TRMM PR resolution. The average rain rate from 0 to 5 km altitude from the TRMM level A25 product [*TRMM*, 2003] is used as input to the model (Figure 1). The model rain height, h, is assumed constant at 5 km. This height has been estimated from the TRMM bright band altitude which can be considered as representative of the freezing level and which is almost constant at 5 km within the TC [*Harris et al.*, 2000]. Figures 3a and 3b present the attenuation and volume scattering terms for the forward look of the inner antenna. For very high rain rate, the attenuation exceeds −20 dB and the volume emission reaches −10 dB. The mean attenuation and volume scattering as a function of rain rate for the two looks and the two incidences, obtained by averaging the data shown Figures 3a and 3b, are presented in Figure 4. These curves are very similar to the model results presented by TQ for analytical rain cells. For rain rates larger than 20 mm hr^{-1}, attenuation is larger than −15 dB; that is, only 3% of the surface backscatter is transmitted back to the sensor through the rain layer, while volume emission exceeds −20 dB. For such occurrences, it is obvious that a correction of the measured NRCS will contain large uncertainties and will be meaningless.

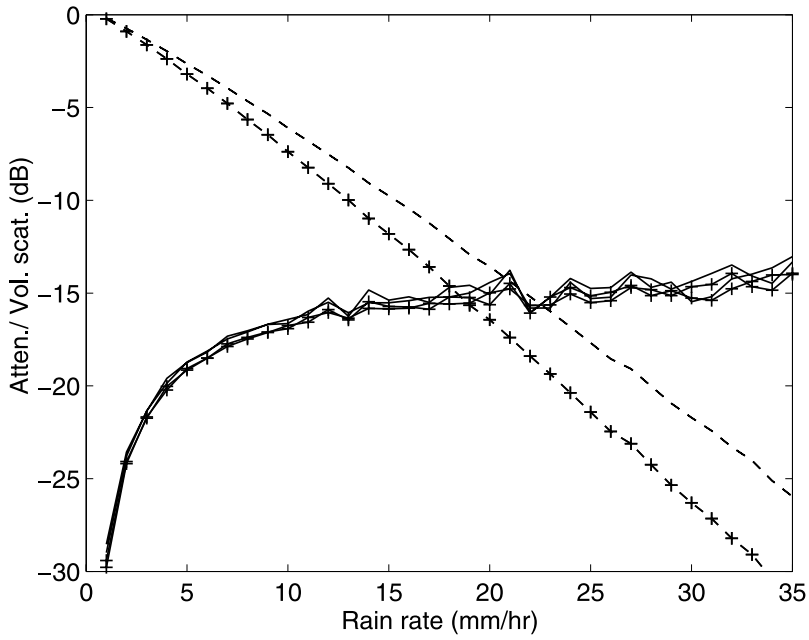

Figure 4. Mean attenuation (dashed lines) and volume scattering (solid lines) as a function of rain rate. Cross-hatched line indicates the outer antenna (V-pol), while the unmarked lines are inner antenna (Hpol).

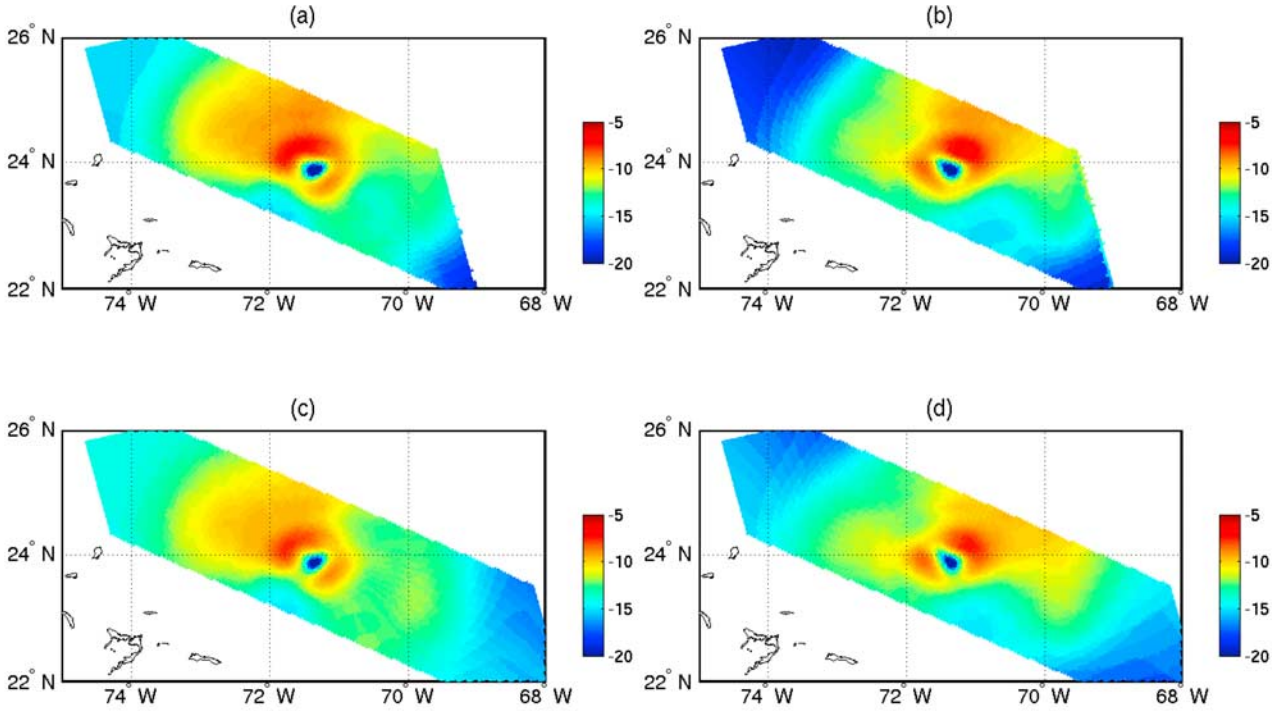

Figure 5. Surface NRCS estimated from the NHC surface wind field of Figure 1b. (a) Inner antenna forward look and (b) aft look. (c) Outer antenna forward look and (d) aft look.

[22] A surface NRCS is computed from the NHC wind field using the KMOD model [*Wentz and Smith*, 1999] and the antenna azimuth and incidence. They are presented in Figure 5. NHC winds are given as maximum 1-min sustained wind speed. To be consistent with the KMOD model function, they are first converted to 10 m 10 min wind speeds using NOAA gust-to-wind conversion charts [*Krayer and Marshall*, 1992]. The modeled NRCS $\widetilde{\sigma}_0$ accounting for rain effects are then computed using equation (12). They are presented in Figure 6. The correlation

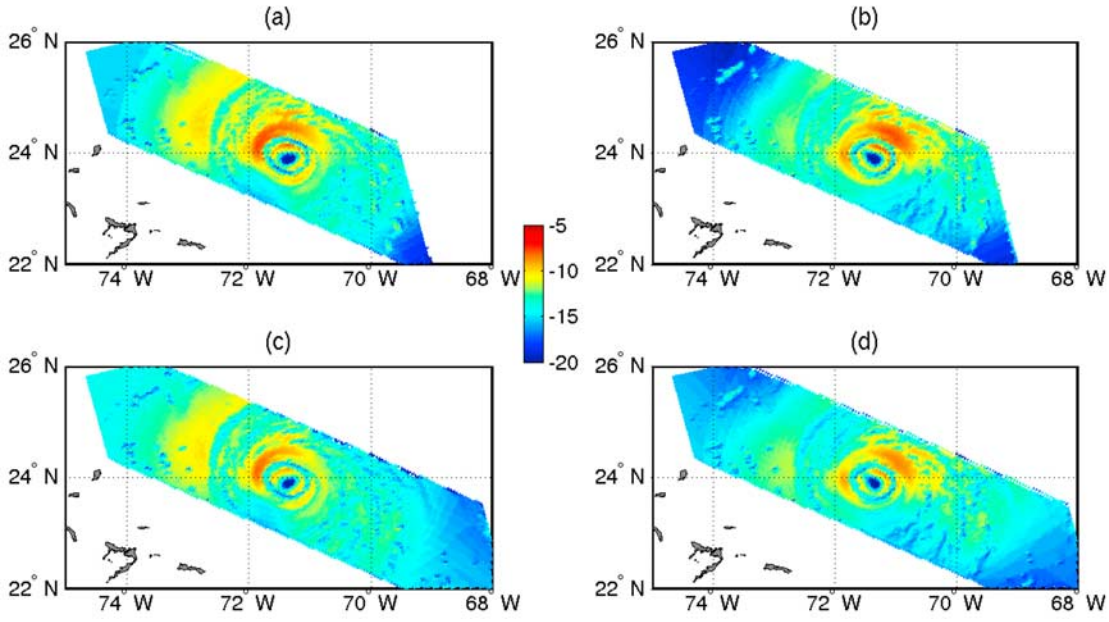

Figure 6. Modeled NRCS for the inner and outer antennae gridded at 4 km resolution on 1048 UT 13 September 1999, using the NHC surface wind field and TRMM rain rate field of Figure 1. (a) Inner antenna forward look, (b) inner antenna aft look, (c) outer antenna forward look, and (d) outer antenna aft look.

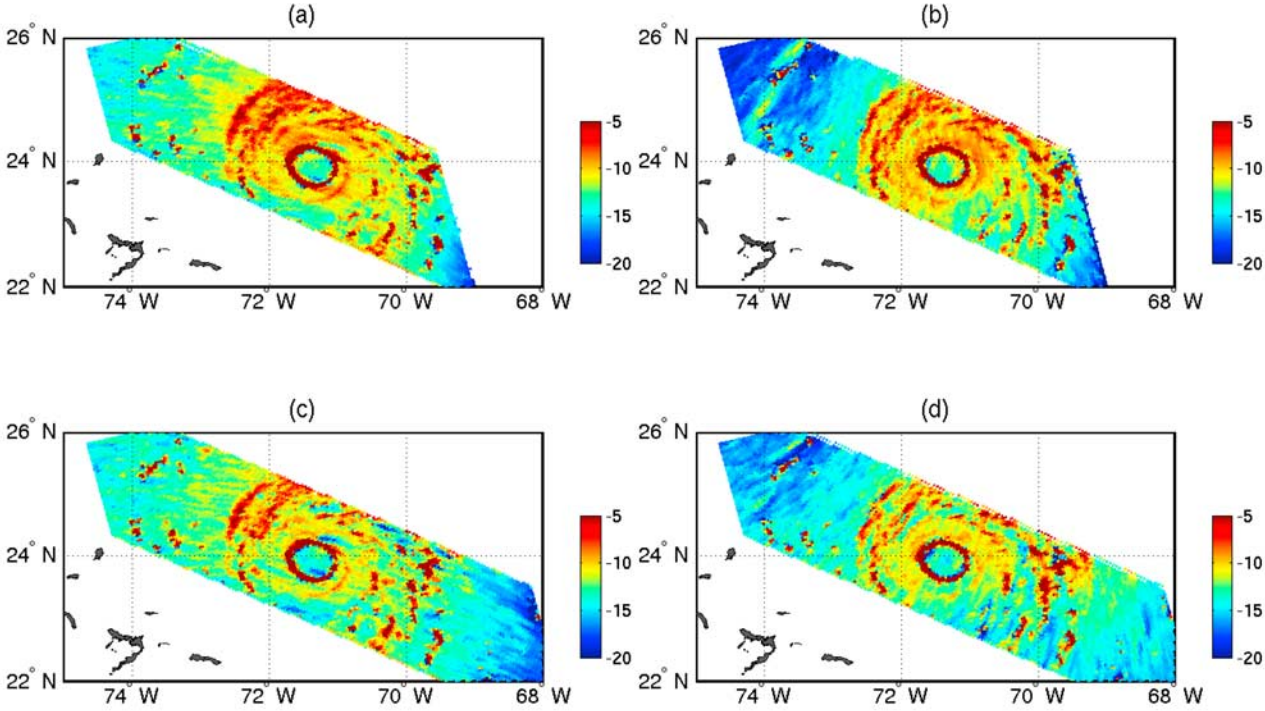

Figure 7. High-resolution corrected NRCS for the inner antenna (a) forward and (b) aft looks and outer antenna (c) forward and (d) aft looks.

between the modeled and measured fields of Figure 2 are, respectively, 62.2%, 74.0%, 61.1%, and 67.8% for the inner and outer antennas and the forward and aft looks. Considering the uncertainties of the different parameters (rain rates, NRCS, KMOD backscattering model, NHC winds) and the time difference between the TRMM and QuikScat data, the patterns of the modeled (Figure 6) and measured (Figure 2) NRCS fields have very similar characteristics, especially near the TC eye, and the fields are well correlated. The results of this forward modeling are good enough to test the correction of the rain influence on the NRCS and the rain flagging procedure.

5.2. Correction of Rain Influence on High-Resolution Measured NRCS

[23] Several studies [*Yueh et al.*, 2001, 2003; *Stiles and Yueh*, 2002] analyzed the effect of rain and proposed rain corrections. However, these corrections were based on coincident low resolution (SSMI) rain rate fields. Following TQ, we analyzed first the correction of high-resolution NRCS fields using high-resolution rain rate fields.

[24] Using equation (12), the linear surface NRCS can be retrieved from the measured NRCS by

$$\sigma_0(x,y) = \frac{\widetilde{\sigma}_0(x,y) - \sigma_{vol}(x,y)}{A(x,y)}. \qquad (17)$$

The four corrected NRCS are thus estimated using the HR measured NRCS and the attenuation and volume scattering terms computed from the TRMM rain field. Using equation (17), negative NRCS values can be found. They correspond to situations where the volume scattering is larger than the measured NRCS. They are associated with either very high rain rates (above 30 mm hr^{-1}) or misplaced rain cells. The numbers of such samples is small (less than 1%), which shows the rather good space/time collocation between the rain rate and NRCS fields.

[25] The HR NRCS corrected for the rain influence are presented in Figures 7a to 7d. They must be compared to the surface NRCS estimated from the NHC wind field presented in Figures 5a to 5d. It is obvious that large differences exist near the eyewall where precipitation are heavy and in the outer region of the TC where some intense rain cells are obviously misplaced and can therefore not be well corrected. It should also be noted that large differences also exist in the area where no rain is present, for example in the northwestern part of the TC. This results certainly from the smoothing effects of the HRD analysis process. However, the general pattern of the surface NRCS, i.e., the wind field structure, is well reconstructed. The correlations of the corrected NRCS fields and surface NRCS fields using NHC wind are 68.1%, 72.0%, 64.8%, and 66.5% for the inner and outer antenna and the forward and aft looks, respectively.

[26] The NRCS correction ranges from −5.6 dB to 15 dB, but only 4% of samples are corrected by more than 5 dB (positive or negative correction) and 8% by more than 3 dB. These relatively small values show that even in extreme events such as tropical cyclones, the strongly inhomogeneous nature of precipitation leads to few samples that are strongly affected by rain at a 4 km resolution. This proportion of samples excessively modified by rain also shows that it could be possible to retrieve useful information on the surface NRCS within wind retrieval cell if the samples too affected by rain were eliminated. Three elimination criteria are considered corresponding to no threshold

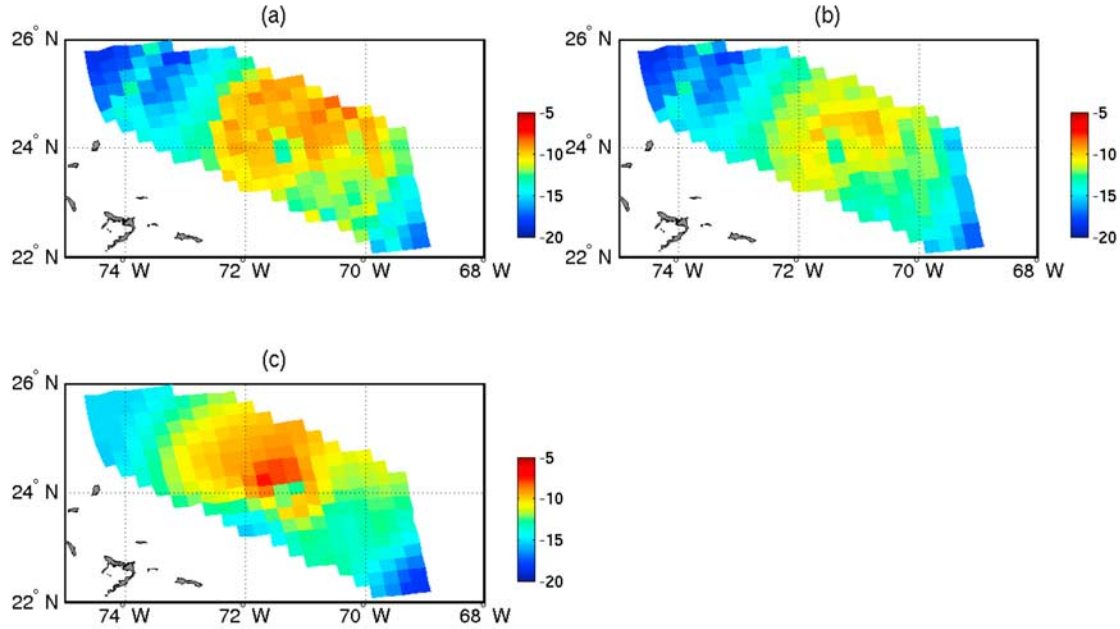

Figure 8. Surface NRCS (inner antenna forward look) averaged over the level 2B data 25 km resolution grid. (a) Corrected using high-resolution data and 3 dB threshold. (b) Uncorrected (level 2B NRCS). (c) Estimated from NHC winds (see Figure 3c).

and 3 dB and 5 dB thresholds on the NRCS HR correction. In the following, they are referred as HR, HR3dB, and HR5dB, respectively.

5.3. Correction of Mean NRCS Within a Wind Vector Cell

[27] As in TQ theoretical study, the corrected HR NRCS fields are averaged over the 25 × 25 km^2 level 2B wind retrieval cells. Three different mean NRCS fields are computed corresponding to the elimination criteria discussed above. The averaged HR3dB corrected NRCS for the forward look of the inner antenna is presented in Figure 8a. For comparison, the averaged uncorrected (level 2B) NRCS and averaged NRCS estimated from the NHC wind fields are also shown in Figures 8b and 8c, respectively. The mean NRCS modification ranges from 0 dB to +2.5 dB. The main effect of rain is thus attenuation as it could be expected for high wind speeds from the results of TQ. The wind speed is everywhere greater than 12 m s^{-1} in the TRMM/QuikScat overlapping area. The figure shows the great improvement of the structure of the NRCS field within the cyclone provided by the HR correction.

[28] The number of samples eliminated by the attenuation thresholds and the mean correction as a function of rain rate are presented in Figure 9a. The small number of samples flagged in the no threshold case corresponds to negative NRCS. For the 3 and 5 dB criteria, the proportion of flagged samples increases steadily from 0% at 0 mm hr^{-1} up to 70% at 20 mm hr^{-1}. The flagging by the two criteria becomes significant for rain rate greater than 3 mm hr^{-1}. The HR3dB and HR5dB corrections have similar shapes and differ sensibly only in the 5–13 mm hr^{-1} range where the maximum difference reaches 0.6 dB. Both mean corrections increase with rain rate up to about 2 dB at 10 mm hr^{-1} (Figure 9b), then decrease slightly and remain almost constant with rain rate. The strong increase of the HR no threshold correction with rain rate shows the impossibility of a pertinent NRCS correction using all the rain-affected samples. It can also be seen as an estimate of the influence of rain at the wind cell resolution. For a 5 mm hr^{-1} rain rate, this correction is above 3 dB and reaches 8 dB for a 10 mm hr^{-1} rain rate.

5.4. Comparison With Low-Resolution Rain Rate Correction

[29] Low-resolution rain data colocated with Seawinds data can be quite easily obtained and several NRCS corrections based on this kind of data have been proposed [*Yueh et al.*, 2001; *Stiles and Yueh*, 2002]. In this section we analyze the validity and pertinence of such correction by comparing the high-resolution correction averaged over a wind resolution cell to the correction estimated from the rain rate, R_{av}, averaged over the same scatterometer cell. Following TQ, the linear correction can be estimated from R_{av} by

$$\widetilde{\sigma_0} = \sigma_0 e^{-2k_a h \sec(\theta)} + \eta \frac{1}{2k_a}\left(1 - e^{-2k_a h \sec(\theta)}\right), \qquad (18)$$

where k_a and η are estimated from R_{av} using equations (7) and (8).

[30] The low-resolution (LR) corrected NRCS are presented in Figure 10. In the eyewall region, equation (18) leads to some negative linear $\widetilde{\sigma_0}$ which are eliminated. Except in the eyewall region, i.e., the region of high averaged rain rate, where the NRCS appear largely overestimated, the overall structure of the NRCS field is sensibly improved by the LR correction. The mean LR correction as a function of rain rate presented in Figure 9b shows that the LR correction underestimates the attenuation and overesti-

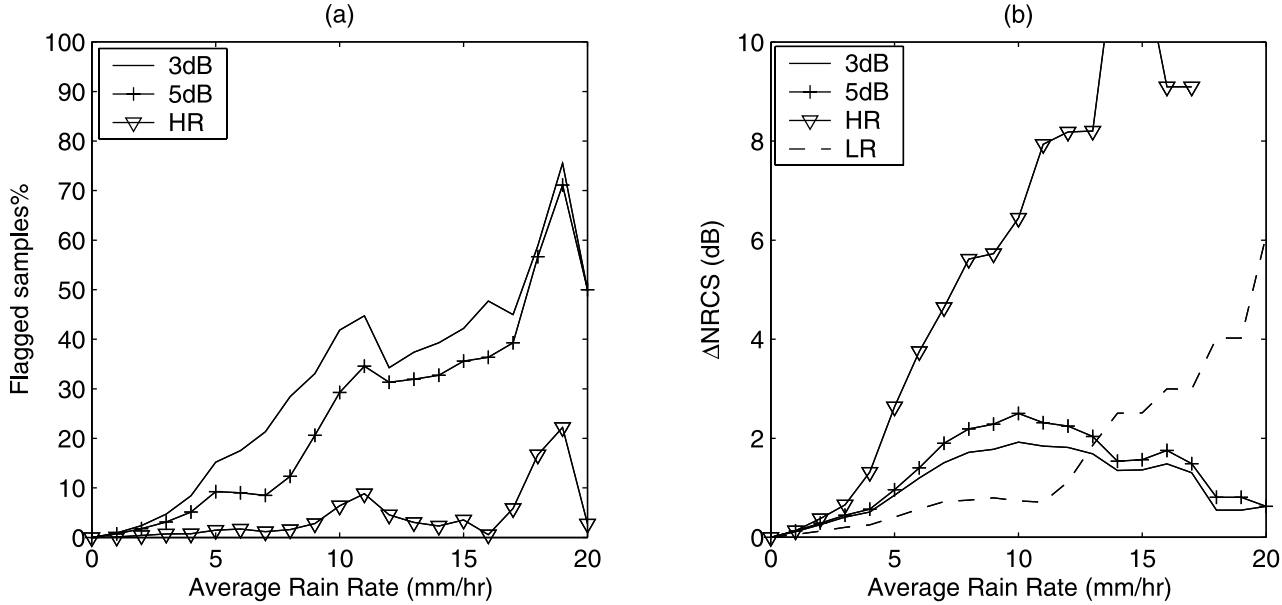

Figure 9. (a) Number of samples flagged by high attenuation criterion as a function of average rain rate and (b) mean correction (Δ NRCS) as a function of rain rate, showing HR 3 dB threshold (solid line), HR 5 dB threshold (crosses), HR no threshold (triangles), and LR (dashed line).

mates the emission especially for rain rates greater than 13 mm hr^{-1}. These results are in good agreement with the TQ theoretical study. For rain rate smaller than 10 mm hr^{-1} the mean LR correction is about 0.5–1 dB smaller than the HR3dB one. For rain rate greater than 13 mm hr^{-1}, in the eyewall region for example, the LR correction becomes several dB larger than the HR3dB one.

5.5. Wind Field Correction

[31] The main purpose of a wind scatterometer is to provide wind vector estimates. These wind data are of particular interest in extreme phenomena such as tropical cyclones which are associated in general with strong rain. In this section, we analyze the correction of the effect of rain on the wind estimates using HR and LR rain rate fields. The NRCS (uncorrected, and HR and LR corrected) are inverted in terms of surface wind vectors using a MLE [*Quilfen and Cavanié*, 1991] and the KMOD model function. To avoid any problem of wind ambiguity removal and for a simpler and more consistent intercomparison of the results, the wind vector solution is sought within ±45° of the 25 km NHC wind direction. The resulting wind vector fields, HR3dB, LR and uncorrected, are presented in Figure 11. The NHC wind fields averaged over the level 2B grid is also shown for comparison. The comparison of the retrieved and NHC averaged wind speeds are presented in Figure 12 as well as the MLE values of the inversion. Table 1 presents the regression coefficients of the Seawinds versus NHC wind speeds, and Table 2 compares HR and LR corrected wind speeds.

[32] Within the region of interest of this study, the operational QuikScat/Seawinds rain flag is set for all the level 2B winds. If the rain flag is considered, no QuikScat data can thus be used to study such phenomenon. Not considering any rain flagging, the level 2B wind speed (see Figure 11) reaches a maximum speed of 33 m s^{-1} well below the 55 m s^{-1} maximum speed of the NHC 25 km averaged field. The north-south asymmetry of the wind field

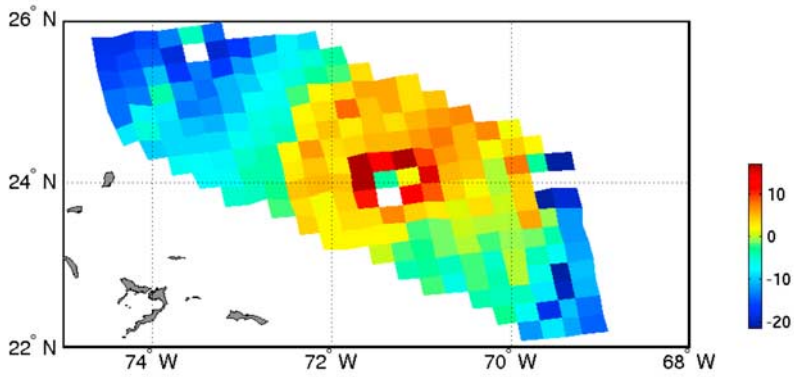

Figure 10. Surface NRCS (inner antenna forward look) averaged over the level 2B 25 km resolution grid and corrected using average rain rate.

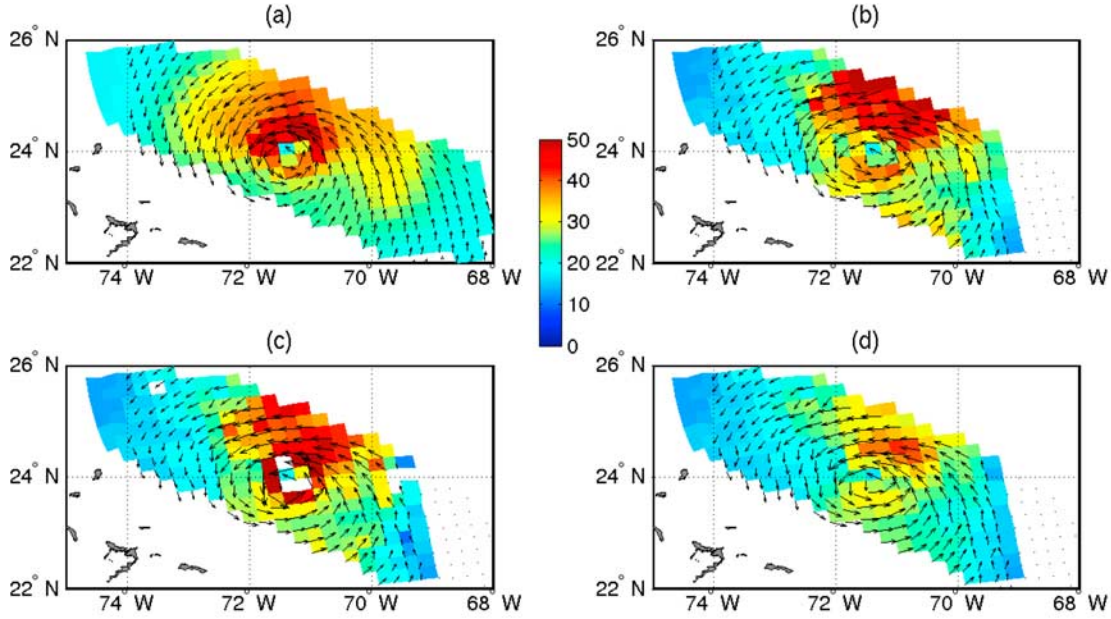

Figure 11. Wind fields comparison. (a) NHC wind field averaged over the 25 km Seawinds level 2B grid. (b) Retrieved wind field using HR 3 dB corrected NRCS. (c) LR corrected NRCS. (d) Uncorrected NRCS.

associated with the rain distribution is strongly smoothed in the level 2B winds. The scatterplots (see Figure 12) and the regression coefficients of the level 2B and NHC averaged wind speed (Table 1) show a strong underestimation of the high wind associated with rain. The error near the cyclone center is about 10–20 m s^{-1}.

[33] Both HR and LR corrections sensibly improve the wind field structure within the TC as well as the wind speed estimates. The zone of maximum wind is better reproduced, except near the eyewall where the precipitations are too intense to allow any NRCS correction. The cyclone entry zone and the north-south asymmetry are also better reproduced. The coefficients of the regression between the QuikScat and the NHC winds given in Table 1 show the significant improvement of the wind speed retrieval, especially for high winds, for all corrections. The regression slope is near unity compared to 0.76 for the level 2B uncorrected wind speeds. As expected, the uncertainties on the rain distribution and the time lag between the two sensors overpasses lead to larger RMS for the corrected winds than that of uncorrected ones. This quite high RMS value (about 5–6 m s^{-1}) has to be put in perspective as the RMS computed for the rain-free samples is about 4 m s^{-1}. The intercomparison of the different corrections (Table 2) shows a high level of consistency with regression slopes around unity and RMS about 1.5 m s^{-1}. The LR correction tends to slightly underestimate high wind speeds because the rain correction is overestimated for high rain rates.

[34] To consider only rain rate smaller than 5 or 10 mm hr^{-1} slightly changes the regression parameters for HR3dB winds. It shows that the criterion used to eliminate samples too affected by rain performs well. The regression parameters are more sensitive to rain rate for HR5dB and LR with lower performances for higher rain rates. The HR5dB and LR corrections perform obviously not as well as the HR3dB one for rain rates larger than 5 mm hr^{-1}. For medium and low rain rates ($\leq$5 mm hr^{-1}), where the threshold criteria eliminate less than 10% of the HR samples, the HR3dB, HR5dB, and LR corrections have similar performances.

[35] This analysis shows that when available, HR rain data can be used to correct measured NRCS and to infer wind speed with an acceptable level of accuracy, even in the presence of intense rain cells if elimination criteria are used. For medium and low rain rates, a LR correction, especially if coincident rain data are available, can also be used efficiently to correct wind fields. However, the MLE, which is a good indicator of the quality of the inversion, is a factor of 2 larger for the LR correction than that of the HR one. Contrary to the HR MLE, which has a similar behavior as the uncorrected one, the LR MLE strongly depends on rain rate. As the rain rate increases, the nonlinearity of the rain influence leads to higher discrepancy between the physics and the model and thus leads to a lesser agreement between the set of NRCS used in the inversion and the model function.

6. Rain Flagging

6.1. Analysis of Operational Rain Flags

[36] Beyond the problem of the correction of rain effects on scatterometer data, which cannot be solved easily, it is of prime importance for operational use and climatological study to efficiently detect the data affected by rain and to determine if a correction is possible. A good flag should eliminate all rain-affected data but should also keep the false alarm rate to a minimum. Currently, two rain indicators are distributed with the level 2B Seawinds wind vectors data [*Jet Propulsion Laboratory*, 2001]. The mp-rain-probability

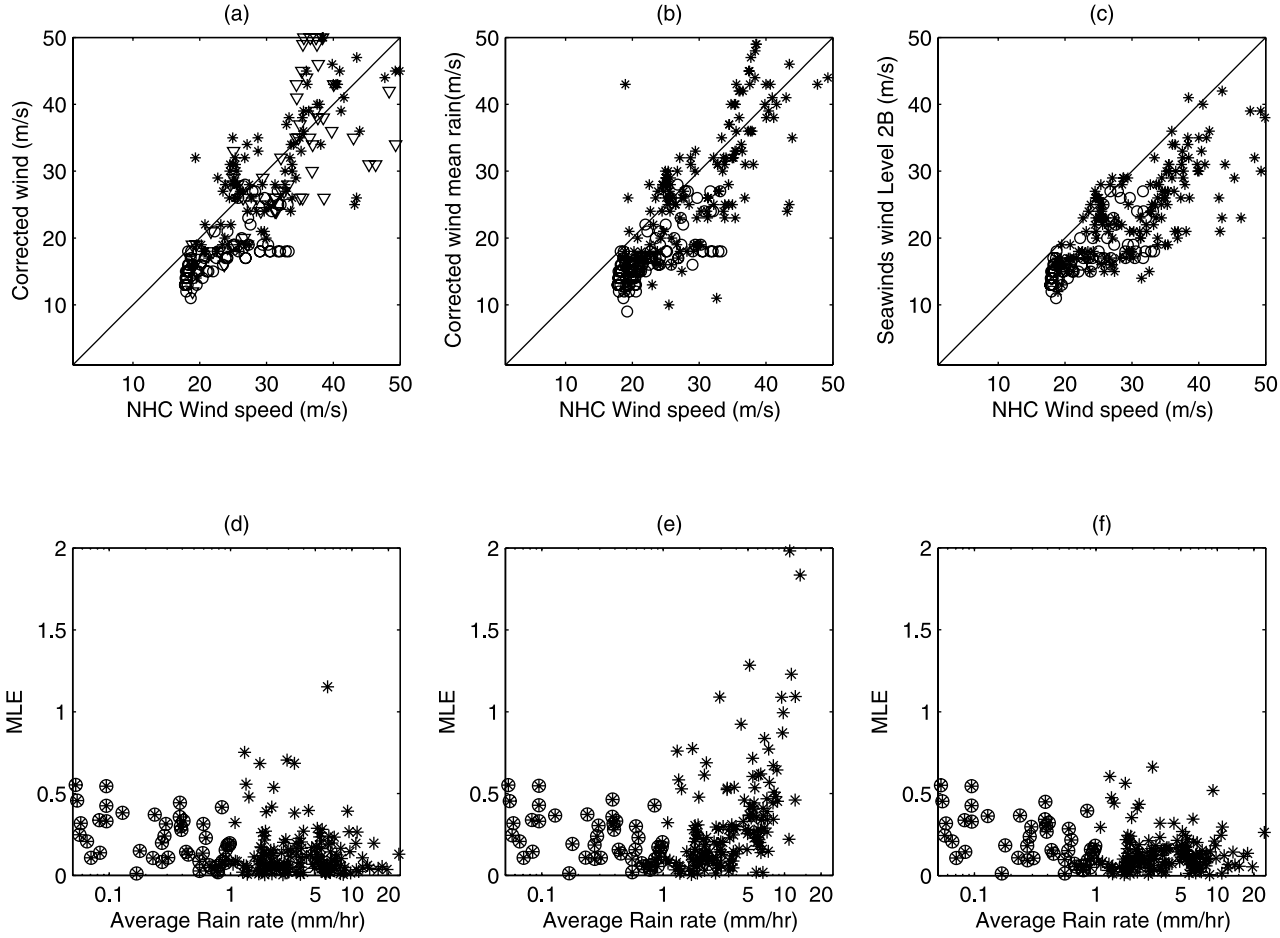

Figure 12. Comparison of retrieved wind speeds: (a) NHC and HR 3 dB wind speed, (b) NHC and LR wind speed, and (c) NHC and uncorrected wind speed. Maximum likelihood estimator as a function of average rain rate: (d) HR 3 dB winds, (e) LR winds, and (f) uncorrected winds. The triangles indicate the winds for which more than 20% of the HR samples are flagged for high attenuation. The circles indicate the nonraining samples.

index is derived using the Multidimensional Histogram (MUDH) rain flagging technique developed by *Huddelston and Stiles* [2001]. It is basically the probability of encountering a columnar rain rate greater than 2 km mm hr^{-1}. This probability is read directly from look-up tables based on several input parameters sensitive to rain including averaged brightness temperature in both H and V polarizations, normalized beam differences, wind speed and direction (relative to along track), and a normalized MLE. The nof-rain-index is based on the Normalized Objective Function (NOF) rain flagging technique developed by *Mears et al.* [1999]. It uses a simplified standard model function to estimate a maximum likelihood estimator and a wind speed for each wind vector cell. This flag is most effective for wind speeds under 10 m s^{-1} and should not be very effective for wind speeds greater than 15 m s^{-1} [*Mears et al.*, 1999]. As it is not presently used for the operational rain flagging and as the wind in the region of study is over 15 m s^{-1}, the NOF rain flag is not considered in this study. Figure 13 presents the MUDH operational rain index as a

Table 1. Regression Parameters of the QuikScat Seawinds Wind Speed to the NHC Averaged Wind Speed[a]

	All Data			$R \leq 10$ mm hr^{-1}			$R \leq 5$ mm hr^{-1}		
Data Set	a	b	RMS	a	b	RMS	a	b	RMS
HR Corr 3 dB	−3.55	1.03	5.77	−3.55	1.03	5.77	−3.55	1.01	5.62
HR Corr 5 dB	−6.38	1.17	6.43	−6.38	1.17	6.43	−4.26	1.04	5.61
LR Corr	−5.72	1.08	5.42	−5.72	1.08	5.42	−3.56	0.97	4.81
Uncorrected	3.20	0.66	4.24	1.88	0.71	4.15	0.82	0.76	4.19

[a]Notation: a, intercept; b, slope.

Table 2. Regression Parameters of the HR Corrected and Uncorrected Wind Speeds to the Low-Resolution Corrected Ones

	All Data			$R \leq 10$ mm hr^{-1}			$R \leq 5$ mm hr^{-1}		
Data Set	a	b	RMS	a	b	RMS	a	b	RMS
HR Corr 3 dB	−0.44	1.06	1.77	−0.44	1.06	1.77	−0.74	1.07	1.49
HR Corr 5 dB	−1.28	1.12	2.52	−1.28	1.12	2.52	−1.01	1.09	1.61
Uncorrected	8.27	0.53	3.38	6.21	0.62	2.59	3.01	0.80	1.19

function of the averaged rain rate R_{av}, and Table 3 presents the probability of detection.

[37] A recent study by *Hoffman et al.* [2004] analyzed in detail the skill of the MUDH rain flag using colocated Seawinds level-2B data, rain rates from meteorological radar, and NCEP mesoscale analysis. They showed that the probability of detection is good for moderate to heavy rain and that for lighter rain the performance degrades. They also found that the rain flag tends to eliminate many high wind speed samples. This confirms earlier results of *Huddelston and Stiles* [2001], who showed that the false alarm rate goes up with the increase in the wind speed. One of the problems when using the MUDH rain flag is the choice of the threshold of mp-rain-probability used to flag the data. A low threshold increases the probability of detection but also increases the false alarm ratio. Two thresholds have been used in this study, the Jet Propulsion Laboratory (JPL) operational one (0.1) and a higher one (0.2) which maximizes the flag skill [*Hoffman et al.*, 2004]. Our analysis of the MUDH rain flag skills confirms these results. The ratio of false alarm is about 56% for the JPL operational threshold and about 10% for the 0.2 threshold. For rain rate below 0.1 mm hr^{-1}, 77% and 70% of the samples are flagged for the 0.1 and 0.2 thresholds, respectively. This proportion exceeds 85% for rain rates above 1 mm hr^{-1} (Table 3). The probability of detection of the MUDH flag is thus very good for rain rate greater 1 mm hr^{-1}. For low rain rate, the detection is good with a score of 60% (75%) for rain rate below 0.4 mm hr^{-1}. The ratio of false alarms strongly depends on the choice of threshold and exceeds 50% for the operational JPL one for high winds.

[38] The MUDH flag is certainly well suited for climatological studies and/or operational use as the probability of nondetection is low. For extreme event analysis, it should be used with caution because of its sensitivity to surface roughness variability within a wind vector cell and its quite high level of false alarm for high winds.

6.2. NRCS Variability as a New Rain Flag

[39] The TQ results on the rain influence showed that the variability of measured NRCS within a wind vector cell is highly sensitive to the rain distribution within the cell. This variability also depends on the wind variability within the cell. In case of low wind speed, i.e., for low NRCS, the rain-induced NRCS variability is 1–2 orders of magnitude larger than the NRCS variability induced by wind-related roughness changes. For high winds, such as the ones encountered in tropical cyclones, the surface roughness variability can be high and could be of the same order of magnitude as the rain-induced variability. It is difficult to model both effects at the same time, but the possibility of rain flagging using NRCS variability can be tested on real data during the Floyd case which presents a wide range of wind speed and rain rates.

[40] The NRCS variability within wind retrieval cell is computed for the two incidences and looks (forward and aft) using the level 1A QuikScat slice data [*JPL*, 2001]. The number of slices data used for the RMS estimation ranges from 16 at nadir to 100 at the outer range for the inner antenna and from 13 to 130 for the outer antenna. Figure 14 presents the maximum of the RMS for the four looks over TC Floyd. The RMS field is clearly correlated to the rain field presented in Figure 1c. The NRCS RMS values increase with the mean rain rate as well as with the rain variability (see Figure 15). The main problem of rain flagging is to define a threshold that can discriminate between the RMS variability resulting from rain or from surface roughness variability. Two orbits intersecting TC Floyd have been thus analyzed using level 1B slice data. The RMS distribution as a function of level 2B wind speed for rain-free (using MUDH rain flag) samples is presented in Figure 15c. The data set contains about 5000 samples. The mean RMS value for rain-free samples is 0.0032 ± 0.0028. The RMS value increases with wind speed to about 0.015 for 20 m s^{-1}. The mean RMS value for samples with rain rate greater than 1 mm hr^{-1} is 0.020 ± 0.006, largely over the value for 20 m s^{-1} winds.

[41] The analysis of the NRCS correction as a function of the NRCS variability (presented in Figure 16) shows that

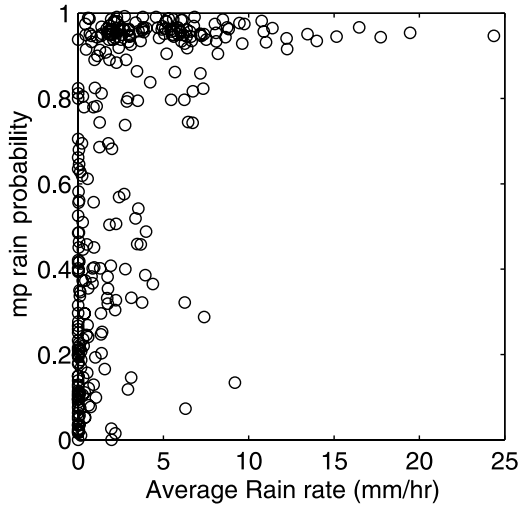

Figure 13. MUDH rain flag analysis: Seawinds level 2B mp-rain-probability as a function of rain rate.

Table 3. Comparison of Rain Flag: Proportion of Rain-Flagged Samples in Percent

	Rain Rate, mm hr^{-1}							
	0	0.1	0.4	1	2	5	10	20
Number of samples	10	27	13	21	33	52	53	13
mp-rain-probability $\geq$ 0.2	10	70	53	85	93	96	98	100
mp-rain-probability $\geq$ 0.1	56	77	75	90	93	97	98	100
NRCS RMS $\geq$ .02	0	22	23	33	51	61	62	92
NRCS RMS $\geq$ 0.015	0	59	61	80	88	92	96	100
NRCS RMS $\geq$ 0.012	63	75	73	90	95	96	96	100

there is a sharp change above 0.012 where the HR correction increases from almost 0 to 4 dB. This confirms the strong correlation between the RMS variability and the influence of rain. The HR3dB and HR5dB corrections steadily increase with increasing RMS and remain below 1 dB for RMS smaller than 0.015. Three RMS thresholds have thus been tested for rain detection: 0.012, 0.015, and 0.02. The skill of the NRCS variability flag to detect rain is presented in Table 3. The 0.012 threshold rain detection probability behaves much like the MUDH rain flag with the JPL threshold with the same probability of rain detection and almost the same ratio of false alarm. The 0.015 threshold has similar performances as the MUDH one with the 0.2 threshold for the rain detection probability but has a much better ratio of false alarm. The 0.02 threshold has a lower detection rate and is certainly not suitable for operational use but certainly set the limit for a possible wind correction. This analysis shows that a low threshold such as the 0.012 one gives similar performance as the MUDH operational one. A higher threshold gives a much better ratio of false alarm with good detection skill and can certainly be used to detect samples affected by rain but that can be efficiently corrected for rain.

[42] As a final example, the NRCS variability rain flag has been applied to the two orbits over flying TC Floyd (about 6000 samples) and compared to the MUHD one. For the first orbit the MUDH (0.2 threshold) index flags 40% of the samples, and the RMS variability index 11% and 18% of the samples at a 0.02 and 0.015 thresholds, respectively. For the second orbit, the proportions are 27%, 1.6%, and 5%, respectively. All the samples flags by the RMS index are also flagged by the MUDH one.

7. Conclusion

[43] In this study, we used colocated high resolution rain data from the TRMM PR radar and high-resolution Seawinds SIR backscatter data to further test and validate the rain-scatterometer interaction model presented in an earlier paper. Using the TRMM rain data as input to the model, the rain attenuation and volume scattering has been estimated within TC Floyd. The results are in good agreement with those of TQ for analytical rain cells. The comparison of measured high resolution SIR backscatter data and synthetic data estimated from the NHC surface winds and the modeled rain terms also showed a good agreement considering the measurement uncertainties and the time lag between the rain and scatterometer data.

[44] The high-resolution modeling also showed that even in extreme rain events such as tropical cyclones, only a few samples are strongly affected (by more than 5 dB) by rain and that it can be possible to correct the wind estimate for rain effects if the samples too affected by rain are eliminated. The correction of the NRCS averaged over wind vector cell has been studied using both high-resolution and low-resolution rain data. High-resolution correction can be used to eliminate rain-affected samples, and a 3dB threshold appears to perform well and to improve significantly the wind retrieval within TC Floyd.

[45] Low-resolution rain data can be also used to correct the average NRCS. In this case, the wind retrieval is also improved. However, the set of corrected NRCS used in the inversion has less physical meaning and thus deviates more significantly from the backscatter model function. This results in larger MLE values that might lead to a flagging

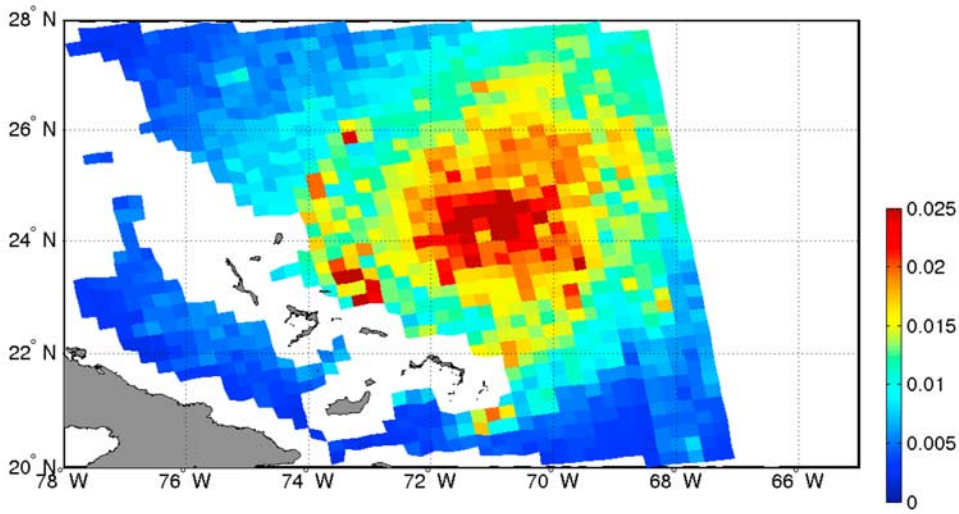

Figure 14. Maximum of the NRCS variability for the two antennae and two looks estimated from the level 1B slices QuikScat/Seawinds data.

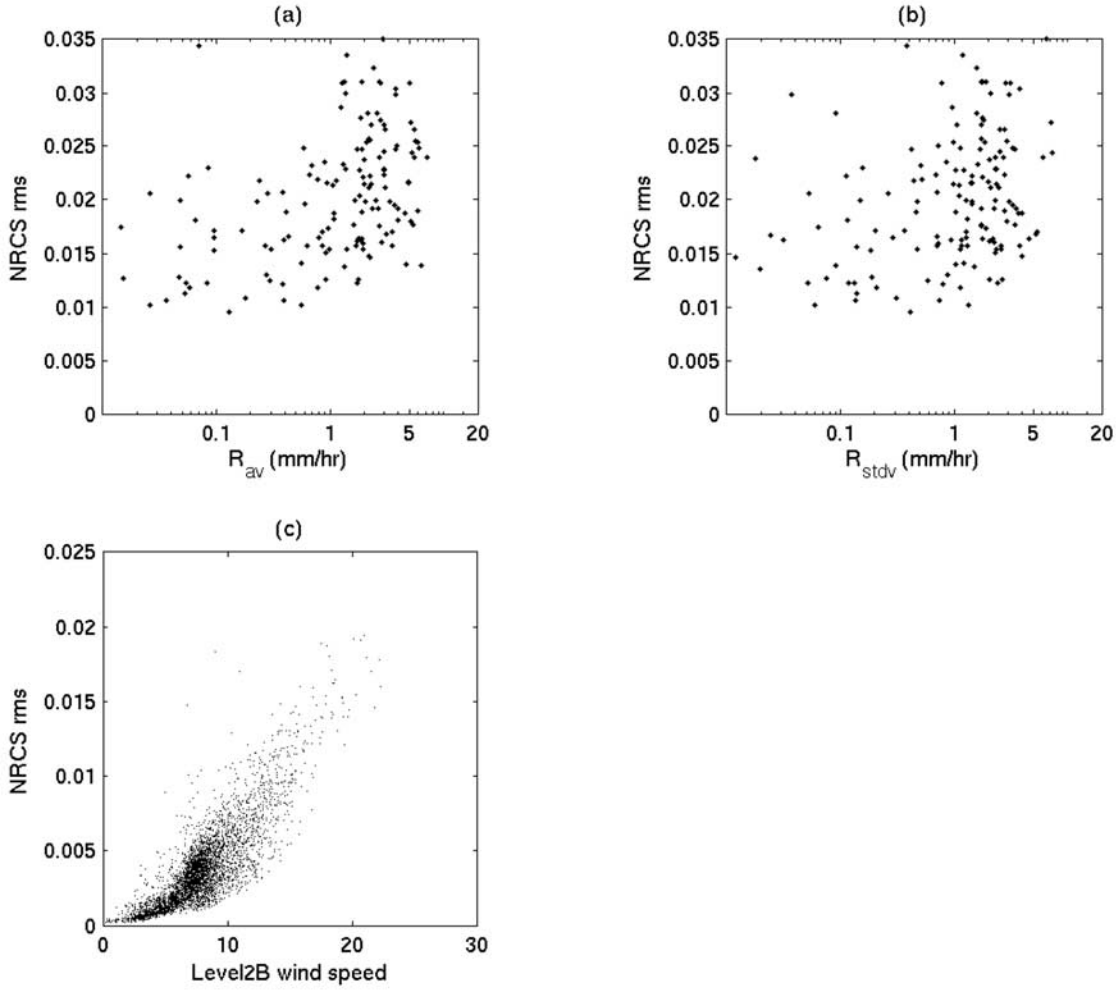

Figure 15. NRCS variability as a function (a) of average rain rate, (b) of rain RMS, and (c) of level 2B wind speed (for rain-free samples).

for bad inversion. However, for rain rates smaller than 5 mm hr^{-1}, this problem is not as crucial and pertinent wind information can be retrieved.

[46] The operational Seawinds rain flag has a good detection skill but has a quite high rate of false alarm, especially for high winds. In case of tropical cyclones, this leads to the elimination of nearly all data within the cyclone. Following the results of the TQ theoretical study, we investigated the skill of a rain flag based on the NRCS variability within a wind vector cell. The RMS of the NRCS is computed from the level 1B slice data for each antenna and each look (forward and aft). This variability strongly depends on the rain distribution but also on the wind speed. However, the analysis of RMS values for rain-free samples shows that except for strong winds (20 m s^{-1}), they are 1 order of magnitude smaller that those of rain-affected samples. Three RMS thresholds have been tested. The lower threshold gives similar results as the operational MUDH one. The middle one has a slightly lower probability of detection for very low rain rate ($\leq$0.4 mm hr^{-1}) but has a much better ratio of false alarm. The higher one can be used to flag samples that cannot be corrected. This kind of rain flag obviously needs further testing in particular under low

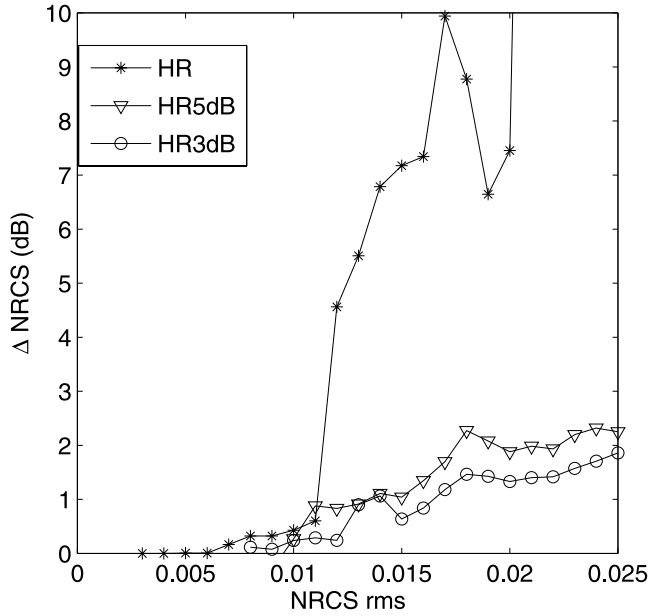

Figure 16. Mean NRCS correction as a function of the NRCS variability for no threshold and 5 and 3 dB thresholds.

wind conditions, but the results are encouraging and show that it can already be used in complement to the operational one.

[47] **Acknowledgments.** The authors are deeply indebted to D. G. Long, who provided the high-resolution QuikScat backscatter data necessary for this study. We also wish to thank the two anonymous reviewers whose comments were of great help in clarifying the text.

References

Bliven, L., P. W. Sobieski, and C. Craeye (1997), Rain generated ring-waves: measurements and modelling for remote sensing, *Int. J. Remote Sens.*, *18*, 221–228.

Contreras, R. F., W. J. Plant, W. C. Keller, K. Hayes, and J. Nystuen (2003), Effects of rain on Ku-band backscatter from the ocean, *J. Geophys. Res.*, *108*(C5), 3165, doi:10.1029/2001JC001255.

Craeye, C., and P. Schlüssel (1998), Rainfall on the sea: Surface renewals and wave damping, *Boundary Layer Meteorol.*, *89*, 349–355.

Draper, D. W., and D. G. Long (2004), Evaluating the effect of rain on Seawinds scatterometer measurements, *J. Geophys. Res.*, *109*, C02005, doi:10.1029/2002JC001741.

Early, D. S., and D. G. Long (2001), Image reconstruction and enhanced resolution imaging from irregular samples, *IEEE Trans. Geosci. Remote Sens.*, *39*, 291–302.

Harris, G. N., K. P. Bowman, and D. B. Shin (2000), Comparison of freezing-level altitudes from the NCEP reanalysis with TRMM precipitation radar bright band data, *J. Clim.*, *13*(23), 4137–4148.

Hoffman, R. N., C. Grassotti, and S. M. Laidner (2004), Seawinds validation: Effect of rain as observed by east coast radars, *J. Atmos. Oceanic Technol.*, *21*, 1364–1377.

Huddelston, J. N., and B. W. Stiles (2001), Multidimensional histogram (MUDH) rain flag: Product description, version 2.1, report, 8 pp., Jet Propulsion Lab., Calif. Inst. of Technol., Pasadena.

Jet Propulsion Laboratory (2001), NASA QuikScat science data product user's manual: Overview and geophysical data products, version 2.1, *JPL Publ. D-18053*, 86 pp., Calif. Inst. of Technol., Pasadena.

Krayer, W. R., and R. D. Marshall (1992), Gust factors applied to hurricane winds, *Bull. Am. Meteorol. Soc.*, *73*, 613–617.

Kummerow, C., W. Barnes, T. Kozu, J. Shiue, and J. Simpson (1998), The Tropical Rainfall Measuring Mission (TRMM) sensor package, *J. Atmos. Oceanic Technol.*, *15*, 809–817.

Marshall, J. S., and W. M. Palmer (1948), The distribution of raindrops with size, *J. Meteorol.*, *5*, 165–166.

Mears, C., F. Wentz, and D. Smith (1999), Special product: Sea winds on QuikScat normalized objective function, report, 13 pp., Remote Sens. Syst., Santa Rosa, Calif.

Melsheimer, C., W. Alpers, and M. Gade (1998), Investigation of multi-frequency multipolarization radar signatures of rain cells over the ocean using SIR-C/X-SAR data, *J. Geophys. Res.*, *103*, 18,851–18,866.

Moore, R. K., Y. S. Mogili, Y. Fang, B. Beh, and A. Ahamad (1997), Rain measurement with SIR-C/X-SAR, *Remote Sens. Environ.*, *59*, 280–293.

Nystuen, J. (1990), A note on the attenuation of surface gravity waves by rainfall, *J. Geophys. Res.*, *95*, 18,353–18,355.

Quilfen, Y., and A. Cavanié (1991), A high precision wind algorithm for the ES1 scatterometer and its validation, paper presented at IGARSS 1991, Int. Geosci. and Remote Sens. Symp., Espoo, Finland.

Slack, J. K., A. R. Holt, and V. Brown (1994), WP 400 workpackage: Implementation of direct algorithms, in *Rain Radar Retrieval Algorithms*, edited by J. Testud, Eur. Space Agency, Noordwijk, Netherlands.

Spencer, M. W., C. L. Wu, and D. G. Long (2000), Improved resolution backscatter measurements with the SeaWinds pencil-beam scatterometer, *IEEE Trans. Geosci. Remote Sens.*, *38*, 2642–2652.

Spencer, M. W., W.-Y. Tsai, and D. G. Long (2003), High resolution measurements with a spaceborne pencil-beam scatterometer using combined range/Doppler discrimination techniques, *IEEE Trans. Geosci. Remote Sens.*, *41*, 567–581.

Stiles, B. W., and S. H. Yueh (2002), Impact of rain on spaceborne ku-band wind scatterometer, *IEEE Trans. Geosci. Remote Sens.*, *40*, 1973–1983.

Tournadre, J., and Y. Quilfen (2003), Impact of rain on scatterometer data: 1. Theory and modeling, *J. Geophys. Res.*, *108*(C7), 3225, doi:10.1029/2002JC001428.

Tropical Rainfall Measuring Mission (TRMM) (2003), *Tropical Rainfall Measuring Mission Science Data and Information System: Interface Control Specification Between the Tropical Rainfall Measuring Mission Science Data and Information System (TSDIS) and the TSDIS Science User (TSU), vol. 4, File Specifications for TRMM Products: Level 2 and Level 3, Release 5.22, TSDIS-P097*, NASA Goddard Space Flight Cent., Greenbelt, Md.

Tsimplis, M. (1992), The effect of rain in calming the sea, *J. Phys. Oceanogr.*, *22*, 404–412.

Ulaby, F. T., R. K. Moore, and A. K. Fung (1981), *Microwave Remote Sensing: Fundamentals and Radiometry*, Artech House, Norwood, Mass.

Wentz, F. J., and D. K. Smith (1999), A model function for the ocean-normalized radar cross section at 14 GHz, *J. Geophys. Res.*, *104*, 11,499–11,514.

Yueh, S. H., B. Stiles, W. Y. Tsai, H. Hua, and W. T. Liu (2001), QuikScat geophysical model function for tropical cyclones and application to hurricane Floyd, *IEEE Trans. Geosci. Remote Sens.*, *39*, 2601–2612.

Yueh, S. H., B. W. Stiles, and W. T. Liu (2003), QuikSCAT wind retrievals for tropical cyclones, *Trans. Geosci. Remote Sens.*, *41*, 2616–2628.

Y. Quilfen and J. Tournadre, Laboratoire d'Océanographie Spatiale, Institut Français de Recherche pour l'Exploitation de la Mer, Technopôle de la Pointe du Diable, F-29280 Plouzané, France. (jean.tournadre@ifremer.fr)